Fault Tolerant Multi-Tx/Multi-Rx Inductive Power Transfer System with a Resonator Coil

Enes Ayaz, Ogün Altun, Hakan Polat, and Ozan Keysan

***Abstract*—This paper presents a novel multi-transmitter (Tx) / multi-receiver (Rx) inductive power transfer system. Compared to conventional single-Tx/single-Rx systems, multi-Tx/multi-Rx topologies increase reliability and fault tolerance. However, unequal power distribution is challenging in these systems due to coupling differences, which prevents them from operating at rated power or requires over-designed modules. This study proposes the addition of a middle-stage resonator (MSR) that balances power distribution by separating direct couplings between Tx and Rx coils. Thus, it increases reliability and fault tolerance. Moreover, an analytical method is proposed to avoid bifurcation, which reduces switching losses. Then, the fault tolerance analysis on multi-Tx/multi-Rx systems and optimum selection of module numbers are investigated. Finally, a 1kW 2Tx/1MSR/4Rx prototype is established to continue operation under single-Tx, single-Rx and double-Rx open circuit faults.**

***Index Terms*—Wireless power transfer, inductive power transfer, modular design, resonator coil, common DC bus, fault tolerance, reliability**

I. Introduction

Inductive power transfer (IPT) systems became prevalent in numerous applications [1]–[5]. They provide cordless, space-free, and reliable solutions to transfer power using the loosely magnetically coupled single-transmitter (single-Tx) and single-receiver (single-Rx) coils [6], [7]. Thanks to their advantages, such as increased transmission distance [8], high misalignment tolerance [9], [10], and fault tolerance [11] compared to single-Tx/single-Rx IPT systems, multi-Tx/multi-Rx systems have recently gained popularity in dynamic applications such as EV chargers, unmanned aerial vehicles, consumer and industrial electronics [12]–[14]. Coupling coefficients and Tx/Rx inductances are time-varying in these dynamic applications [15], resulting in a change in the resonant frequency, power, and efficiency, which in turn result in reliability and fault issues.

Multi-Tx/multi-Rx systems provide flexible mobility, and they can supply rated power with higher efficiencies even if transmitters and receivers are misaligned [16]–[18]. They create modular structures, and the system can transfer rated power under faulty conditions. Besides, power ratings of these IPT systems can be increased just by increasing the number of Tx/Rx coils, and the current and voltage ratings can be adjusted via the number of series/parallel connections of modules [19]–[21].

Enes Ayaz, Ogün Altun, H. Polat and Ozan Keysan are with Middle East Technical University, Department of Electrical and Electronics Engineering, Ankara, Turkey. Email: keysan@metu.edu.tr

Corresponding Author: Ozan Keysan, keysan@metu.edu.tr

Multi-Tx/multi-Rx systems have power-sharing issues due to coupling differences coming from the nature of dynamic applications, which causes early aging modules and reliability problems [22], [23]. The conventional solution is to over-design the system. Otherwise, unequal power distribution can exceed the voltage/current ratings of the modules. Alternatively, an active full-bridge converter can be used on the receiver side instead of the diode rectifier to equalize the power distribution, increasing cost and complexity. Moreover, based on the electrical connections of multiple modules, the compensation methods also affect the power distribution [24]. Therefore, choosing a reasonable compensation method can improve power-sharing, but this may distort other factors, such as coupling factors, resonant frequencies, etc. Another issue is to design bifurcation-free multi-Tx/multi-Rx systems. The bifurcation phenomenon may arise in doubly compensated systems in relation to the coupling and load conditions, yielding more than one zero phase angle (ZPA) and distorting zero voltage switching (ZVS) above the resonant frequency [25]. Since ZVS helps to reduce the switching losses, a bifurcation-free design is preferred for higher efficiency. Compared to single-Tx/single-Rx systems, a bifurcation-free multi-Tx/multi-Rx system design is complex compared to single-Tx/single-Rx systems. Although systematic design guidelines have been presented for single-Tx/single-Rx [26], a general systematic design for multi-coil systems is not studied in the literature.

In this paper, a multi-Tx/multi-Rx IPT system is introduced for dynamic applications. In order to solve the power-sharing issue, a middle-stage-resonator (MSR) coil is proposed, which is cost-efficient and simplifies operation under fault. Also, an analytical design methodology is proposed to avoid the bifurcation phenomenon, increasing transfer efficiency. The rest of the paper is organized as follows. Section II shows the system structure and problem definitions. In Section III, the bifurcation free-design methodology is given. Section IV presents the analytical analysis of fault tolerance. In Section V, experimental verification is made for a 2Tx/1MSR/4Rx system.

II. System Structure and Problem Definition

The prototype in this paper is designed as a contactless slip ring to replace conventional slip-rings for large synchronous generators' (SG) field excitation. Conventional slip rings require regular maintenance, raising reliability and fault tolerance issues and increasing operating costs. In order to solve these problems, a multi-Tx/single-MSR/multi-Rx IPT system is proposed, as shown in Fig. 1.a. Tx modules, MSR,

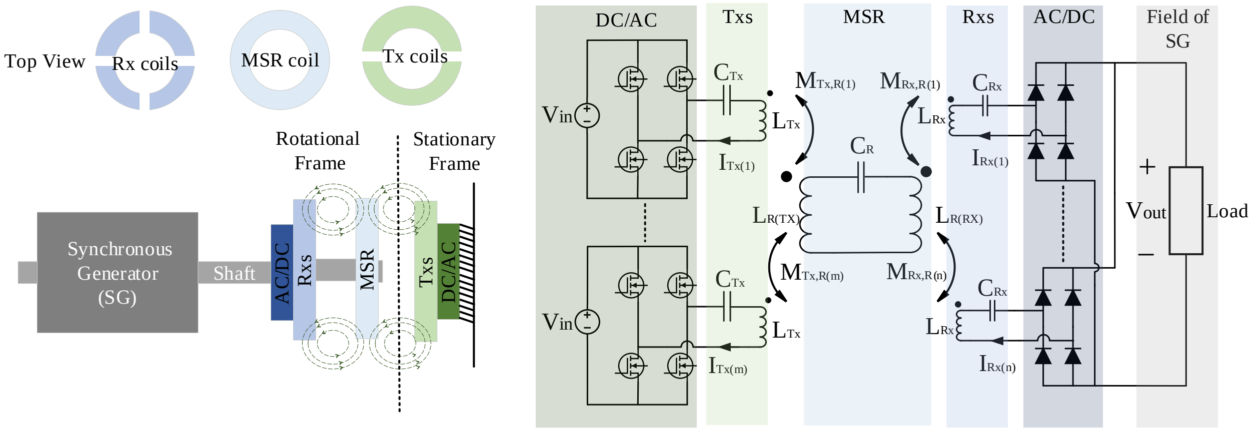

(a) (b)

Fig. 1. The proposed multi-Tx/multi-Rx system with a middle-stage-resonator (MSR). a) Representation of the proposed system. b) Circuit diagram of the proposed system.

and Rx modules are placed around the rotating shaft. The Rx modules and MSR rotate with the shaft while the Tx modules are on the stationary frame. Therefore, Rx and MSR coils are relatively stationary, which means their magnetic couplings are constant during rotation. However, magnetic couplings between Tx and the resonator coils change with rotation. The Tx side consists of full-bridge converter modules. The Rx side is uncontrolled and contains passive full-bridge diode rectifiers to reduce the complexity. Rx modules are connected in parallel, and the common DC output is connected to the field winding of the SG as shown in Fig. 1.b.

A. Problem Definition

The couplings between Tx and Rx modules vary with the position of the shaft. The series-series (SS) compensation method is selected to keep the resonant frequency constant with the rotation as presented in [27]. However, a significant problem of SS compensation is the lack of operation under zero coupling [28], and the large induced currents in the Tx side under light-loaded/open-circuited cases. Furthermore, coupling coefficients vary during rotation, and overcurrent is the potential source of failure in light-load conditions, damaging semiconductor devices. For a reliable and fault-tolerant operation, the system should operate under open-circuit faults. Therefore, the Rx modules are connected in parallel to isolate the faulty open-circuited module from the others.

B. Multi-Tx/Multi-Rx coils without the MSR coil

In multi-coil systems, coupling factors between Tx and Rx modules vary with rotation. The unequal power-sharing problem occurs in Rx modules due to magnetic coupling differences and passive diode rectifiers. The diode rectifier of the module with higher coupling blocks the other modules, so the majority of power is transferred over a single module. As an example, the current distribution of a 2Tx/4Rx system is shown in Fig. 2 for equal and unequal couplings.

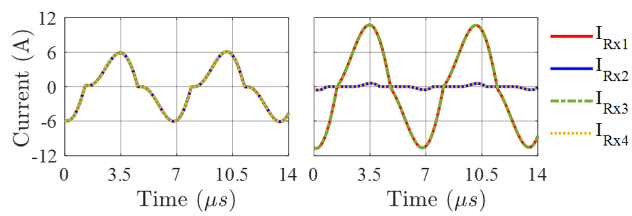

(a) (b)

Fig. 2. Rxs' current distributions. a) Equal couplings between Txs and Rxs. b) Unequal couplings between Txs and Rxs.

C. Addition of a MSR coil

Introducing an MSR eliminates the direct couplings between Tx and Rx modules. Since MSR and Rxs are relatively stationary, the couplings between resonator and Rx does not vary with rotation. Although couplings between Txs and the MSR coils change with rotation, this does not affect the current distribution of Rxs. They create unequal power distribution between Txs, which the active full-bridge converter can mitigate. As a consequence, the addition of an MSR isolates Txs and Rxs. An example, the 2Tx/1MSR/4Rx system is shown in Fig. 3 for equal and unequal couplings between the MSR and Txs.

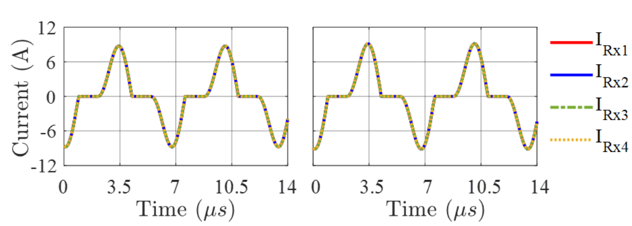

(a) (b)

Fig. 3. Rxs' current distributions of 2Tx/1MSR/1Rx. a) Equal couplings between Txs and Resonator. b) Unequal couplings between Txs and Resanotor.

III. DESING METHODOLOGY OF BIFURCATION-FREE SYSTEM WITH AN MSR

A. Critical Coupling for Bifurcation Limits

In the proposed system, the Tx and Rx sides are decoupled. The power is transferred with a resonator coil placed between the Tx and Rx coils. The system will be analytically designed for single-Tx/single-Rx with an MSR as presented in Fig. 4.a, and then it will be extended to a multi-Tx/multi-Rx system.

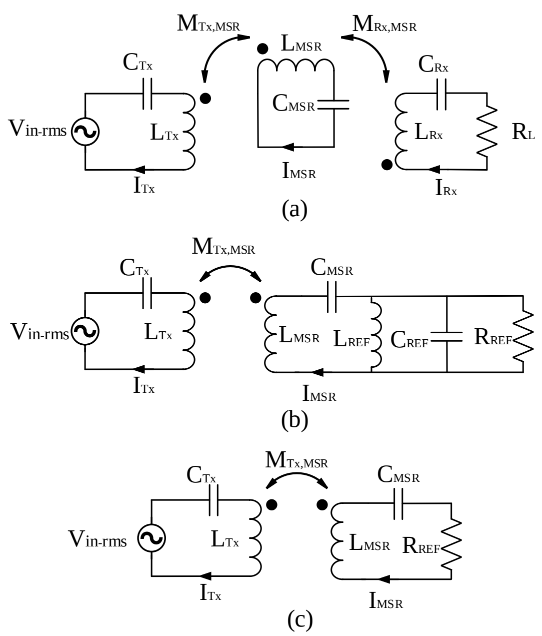

Fig. 4. The circuit representations. a) 1Tx/1MSR/1Rx System. b) Reflected Rx side on the MSR. c) Reduced reflected low quality Rx side on the MSR.

The reflected impedance of Rx modules on the MSR, denoted by Z_{ref}, is obtained by (1).

$$Z_{ref} = \frac{\omega^2 M_{R,Rx}^2}{j\omega L_{Rx} + \frac{1}{j\omega C_{Rx}} + R_L} \tag{1}$$

Although Rx modules are compensated by SS, Z_{ref} can be modelled by parallel resonant circuits L_{Ref}, C_{Ref}, R_{Ref} as given in Fig. 4.b. The reflected parallel resonance circuit impedance could be written as in (2).

$$Z_{ref} = \frac{1}{\frac{1}{j\omega L_{ref}} + j\omega C_{ref} + \frac{1}{R_{ref}}} \tag{2}$$

By using (1) and (2) L_{ref}, C_{ref} and R_{ref} can be found as in (3) where $\Phi = \omega^2 M_{R,Rx}^2$.

$$L_{ref} = \Phi C_{Rx}, \quad C_{ref} = \frac{L_{Rx}}{\Phi}, \quad R_{ref} = \frac{\Phi}{R_L} \tag{3}$$

If the quality factor of the reflected parallel resonant is high enough, the reflected impedance can be assumed to be resistive; thus, it can be reduced to a conventional SS system as shown in Fig. 4.c. The higher quality factor of reflected parallel resonant means the lower quality factor of Rx modules, which can be found by (4).

$$Q_{Rx} = \frac{\omega L_{Rx}}{R_L} = \frac{1}{\omega C_{Rx} R_L} \tag{4}$$

Choosing a lower Rx's quality factor by increasing Rx's capacitance results in only a resistive component on the resonator side. Hence, bifurcation-free design can be achieved by adjusting the quality factor of a resonator with reflected resistance, as given in (5).

$$Q_{MSR} = \frac{\omega_0 L_{MSR}}{R_{ref}} \tag{5}$$

Thus, the critical coupling between the Tx coil and the resonator coil can be formulated as in (6), which has been derived in [26], [29].

$$k_c = \frac{1}{Q_{MSR}} \sqrt{1 - \frac{1}{4Q_{MSR}^2}} \tag{6}$$

B. Design Methodology of Single-Tx/Single-MSR/Single-Rx System

In order to obtain a systematic design, the flow chart in Fig. 5 is established. The system is designed as single-Tx/single-Rx, and the effect of the number of modules will be discussed in the following section. Firstly, input power, DC input voltage, DC output voltage, resonant frequency, and load resistance are selected as the initial parameters.

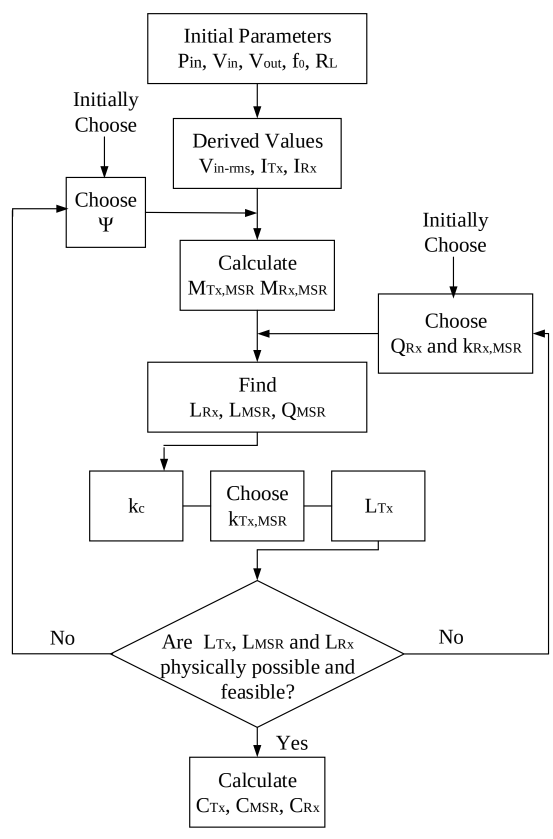

Fig. 5. Flowchart of the proposed design.

After that, the AC input voltage, transmitter current (with single-Tx), receiver current (with single-Rx) are derived from the initial parameters, as in (7).

$$\begin{aligned} V_{in-rms} &= \frac{2\sqrt{2}}{\pi} V_{in} \\ I_{Tx} &= \frac{\pi}{2\sqrt{2}} \frac{P_{in}}{V_{in}} \\ I_{Rx} &= \frac{\pi}{2\sqrt{2}} \frac{P_{out}}{V_{out}} \end{aligned} \tag{7}$$

The ratio of the MSR and the transmitter currents (Ψ), shown in (8), is a design parameter that changes the resonator coil size and copper losses. Increasing Ψ decreases the MSR's size but increases the resonator current, which raises the copper losses. The coil sizes of the MSR and transmitter become closer if Ψ is chosen near unity.

$$\Psi = \frac{I_{MSR}}{I_{Tx}} \tag{8}$$

At the resonant frequency, the induced voltage on the Tx coil is equal to the input voltage. Hence the mutual inductance between Tx and MSR coils can be calculated as in (9).

$$M_{Tx,MSR} = \frac{V_{in}}{\omega_0 I_{MSR}} \tag{9}$$

A similar approach can be made for the mutual inductance between the MSR and Rx side coils as in (10).

$$M_{Rx,MSR} = \frac{V_{out}}{\omega_0 I_{MSR}} \tag{10}$$

Then, the coupling factor between the MSR and Rx coils ($k_{RX,MSR}$) and the quality factor of Rx (Q_{Rx}) are chosen which should be relatively lower, as discussed previously. Furthermore, $k_{RX,MSR}$ does not affect the bifurcation. Higher $k_{RX,MSR}$ requires the air gap between these coils to be small, which decreases the size of the MSR coil. Hence, the values should be chosen considering the application and mechanical limits. Accordingly, the Rx side inductance can be calculated as in (11) where R_{equ} is the equivalent resistance, as seen from the diode rectifier on the Rx side, and the MSR inductance is calculated as in (12).

$$L_{Rx} = \frac{Q_{Rx} R_{equ}}{\omega_0} \tag{11}$$

$$L_{MSR} = \frac{M_{Rx,MSR}}{k^2_{Rx,MSR} L_{Rx}} \tag{12}$$

Thus, the quality factor of the MSR (Q_{MSR}) is found by R_{equ} and L_{MSR} as given in (13).

$$Q_{MSR} = \frac{\omega_0 L_{MSR}}{R_{ref}} = \frac{\omega_0 L_{MSR}}{\dfrac{\omega_0^2 M^2_{Rx,MSR}}{R_{equ}}} \tag{13}$$

Q_{MSR} determines the critical coupling, assuming a low enough Rx quality factor. The coupling between Tx and the MSR ($k_{Tx,R}$) is chosen below the critical coupling to achieve a bifurcation-free design, and the Tx side coil inductance can be calculated as in (14).

$$L_{Tx} = \frac{M_{Tx,R}}{k^2_{Tx,MSR} L_R} \tag{14}$$

All three coils are adjusted to have the same resonant frequency and hence the C_{Tx}, C_R and C_{Rx} can be calculated as in (15).

$$\begin{aligned} C_{Tx} &= \frac{1}{L_{Tx}\omega_0^2} \\ C_{MSR} &= \frac{1}{L_R\omega_0^2} \\ C_{Rx} &= \frac{1}{L_{Rx}\omega_0^2} \end{aligned} \tag{15}$$

C. Expansion to Multi-Tx/Multi-Rx System

Single-Tx/Single-MSR/Single-Rx design steps can be expanded to a multi-Tx/single-MSR/multi-Rx system, in which the only difference is that input and output currents are shared between the modules. On the one hand, the number of Rxs does not affect the design steps. Each Rx has a multiplied load resistance with the number of Rx modules, shown in (16), because the Rxs are connected to a common DC-Bus via a passive diode rectifier.

$$R_{L(Rx)} = n(R_L) \tag{16}$$

The total reflected resistance on the MSR is calculated as given in (17).

$$R_{ref} = \sum_{i_1}^{i=n} \left(\frac{\omega^2 M^2_{Rx,MSR}}{n(R_L)} \right) = \frac{\omega^2 M^2_{Rx,MSR}}{R_L} \tag{17}$$

Since the reflected resistance is independent of the number of Rx, the system can be designed as a 1Rx, and the same derived parameters can be used in multi-Rx, regardless of the number of modules.

On the other hand, the number of Tx modules affects the design steps. The reflected resistance on the Tx module is given in (18).

$$R_{Ref-Tx} = \frac{\omega^2 M^2_{Tx,MSR}}{R_{Ref}} \tag{18}$$

Although the reflected resistance is independent of the number of Tx modules, the power of each Tx is the input power divided by the number of Tx modules. Thus, a single-Tx/single-MSR/single-Rx can be designed by reducing the input power per Tx module, and the derived parameters are used in multi-Tx systems.

IV. Fault Tolerance Analysis

This section will discuss the effect of the modules number on the system fault tolerance. Although using more modules increases fault tolerance, the physical limitation of the modules and cost determine the optimum number of the modules. There are m Txs and n Rxs where the physical placement of example 2Tx/1MSR/4Rx coils are presented in Fig. 6.

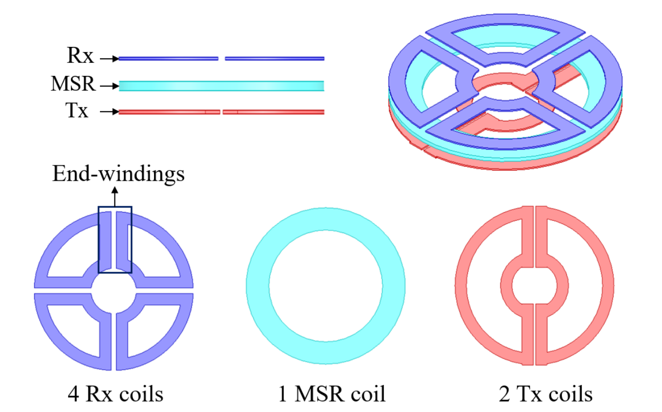

Fig. 6. The coil placements of the proposed multi-Tx/1-MSR/multi-Rx (as an example 2Tx/1MSR/4Rx) system. (For visual clearity, only coils are shown.)

The load resistance is assumed to be constant as it is a field resistance of an SG. Firstly, assuming that i numbers of Tx modules are damaged and they turn in open-circuit. At this point, the induced voltage on the load decreases as given in (19).

$$V_{L-faulty} = V_L \left(\frac{m-i}{m} \right) \tag{19}$$

On the one hand, increasing the number of Tx modules makes the power transfer capability rise under a single Tx fault, which results in that the more modules there are, the more fault-tolerant the system is. On the other hand, the placement of the coils becomes more challenging in every step to increase the module number because the coils' end-windings reduce the effective area of the coils and decrease the mutual inductances. In order to increase the number of modules, the required space increases, and the system becomes unfeasible.

Secondly, assuming that i numbers of Rx modules are in open-circuit fault, it is observed that the reflected resistance on the resonator is independent of the faults, as given in (20).

$$R_{Ref-faulty} = (n-i) \left(\frac{\omega^2 M_{RX,MSR}^2}{(n-i) R_L} \right) = \frac{\omega^2 M_{RX,MSR}^2}{R_L} \tag{20}$$

From Txs' point of view, there is no change in their current and voltage. However, the currents on the Rx modules become larger, and they should be limited to their ratings. Therefore, the transferred power decreases, as given in (21).

$$P_{out-faulty} = P_{out} \frac{(n-i)^2}{n^2} \tag{21}$$

If modules are over-designed, it is possible to transfer rated power under faulty conditions. Over-design ratio along with the number of modules to provide constant power under fault conditions are shown in Fig. 7. Increasing the number of modules decreases the overdesign percentage. It makes the system more reliable and fault-tolerant but raises the cost and complexity and creates sizing problems.

The benefits of increasing the module number saturate after some point, whereas the required space and cost continue to increase. For instance, four modules are enough for a single

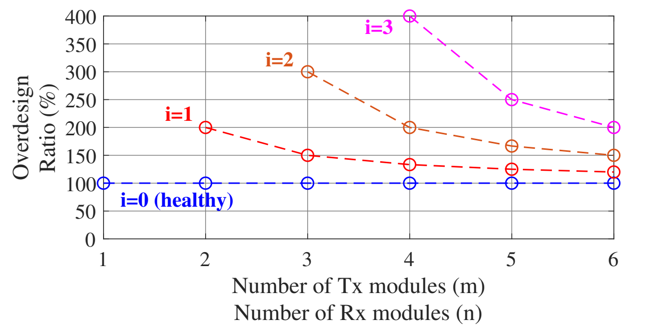

Fig. 7. Over-design rating of each module to transfer the rated power under faulty condition. (i: number of faulty modules.)

module fault, as can be seen in Fig. 7. Therefore, we design an example system with 2-Tx and 4-Rx where the parameters are given in Table I.

TABLE I
2Tx/1MCR/4Rx IPT System Design Parameters and

Fixed Parameters		Derived Parameters	
Power Rating	1000 W	Power per Tx	500 W
Input Voltage V_{in}	100 V_{DC}	$k_{cTx,R}$	0.2382
Output Voltage V_{out}	110 V_{DC}	$M_{Tx,R}$	15.62 μH
Resonant Frequency f_r	150 kHz	$M_{Rx,R}$	17.36 μH
Load Resistance R_L	10 Ω	L_{Rx}	25.47 μH
Number of Txs m	2	L_R	73.98 μH
Number of Rxs n	4	Q_R	4.167
Ψ	1.1	L_{Tx}	82.51 μH
Q_{Rx}	1.5	C_{Tx}	13.60 nF
$k_{Rx,R}$	0.4	C_{Rx}	44.20 nF
$k_{Tx,R}$	0.2	C_R	15.21 nF

V. Simulation Results and The Feasibility of Analytical Model

The analytical model may deviate due to the assumptions such as reduced reflected impedance under the low-quality factor and the first harmonic approach (FHA) used in the analytical model. In this section, the deviations will be investigated, and the effect on the bifurcation phenomena and output voltage gain is analyzed.

A. Critical Coupling Limitations

In this part, the critical coupling calculated by the analytical model is compared with simulation results to validate the analytical model, which should guarantee the bifurcation-free operation. The analytical design procedure is repeated along with $Q_{RX} = 0.2$ to $Q_{RX} = 2.2$. For $k_{Rx,R} = 0.4$ and $\Psi = 1.1$, the critical couplings are calculated by both analytical and simulation models. As can be seen in Fig. 8, the analytical results deviate from the simulation for higher Q_{Rx} (> 1) values. The deviation can be ignored due to the critical coupling of the analytical model is always smaller than the simulation results. Therefore, the selected coupling below the critical value calculated by the analytical model always gives a bifurcation-free system.

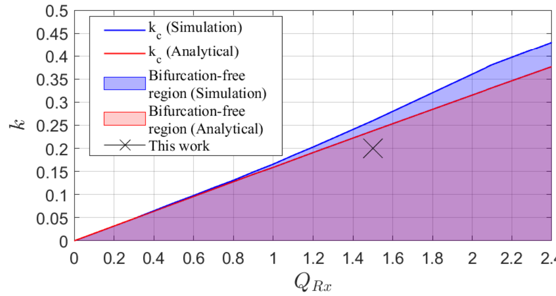

Fig. 8. Comparison of critical couplings for different Q_{RX} values.

B. The Effect of Diode Rectifier

In this part, the voltage gain calculated by the analytical model is compared with the simulation results. The analytical design methodology is based on fundamental harmonic approximation (FHA), which is presented under these assumptions: no-higher order harmonics and continuous coil current, also known as continuous current mode (CCM) [30]. However, an IPT system can also operate in discontinuous current mode (DCM) because of the diode rectifiers and the low-quality factor of Rx modules [31]. In DCM, the currents of the coils have odd harmonics (3^{rd}, 5^{th}), which are comparable to the fundamental component. In our system, we observe DCM operation where the current waveforms are shown in Fig. 9.

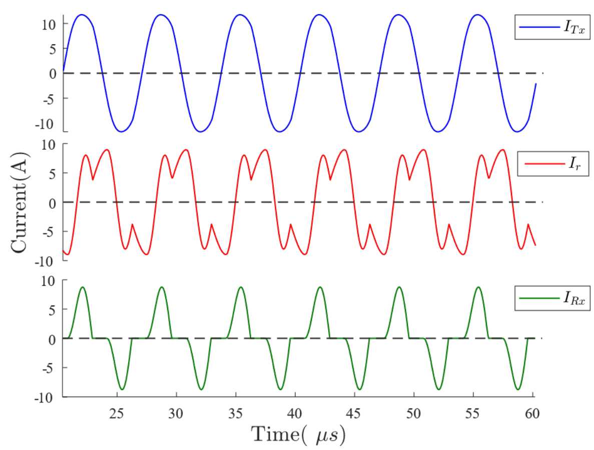

Fig. 9. 1Tx-1R-1Rx current waveforms during DCM operation.

Thus, the analytical model deviates due to the DCM operation, and it also causes the voltage gain to increase due to third harmonics. The design procedure is repeated along with different Q_{Rx}, as shown in Fig. 10. The voltage gain is 10% greater than the analytical calculation for our system due to DCM operation. However, this deviation can be tolerated since it does not affect the critical couplings.

VI. Experimental Results

To verify the proposed system, a 1 kW 2Tx/1MSR/4Rx prototype is built as shown in Fig. 11. The parameters of the experimental setup are shown in Table II. In order to achieve high fault tolerance, Rx modules are over-designed, which provides the system to transfer rated power under Rx faults.

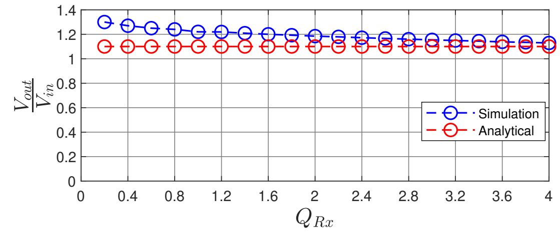

Fig. 10. The voltage gain over different Q_{Rx} for FHA based analytical model and simulation results with DCM operation.

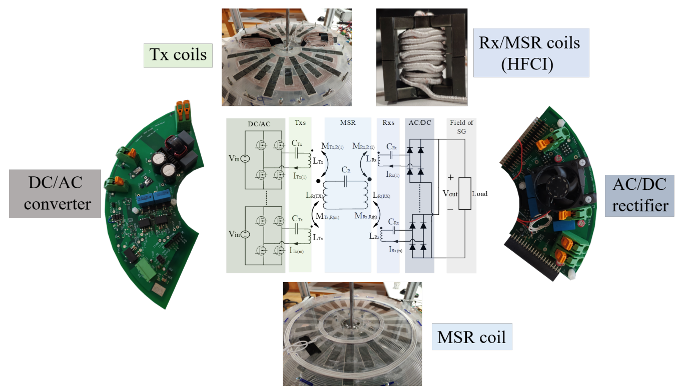

Fig. 11. Experimental setup for the proposed IPT system [29]

A. IPT Coil Design Considerations

Unlike most IPT systems, the air gap of the proposed system is under the designer's control. In the proposed system, the couplings between Tx and Rx coils are eliminated, and so the MSR coil is separated into five coils that are connected in series, where one coil couples with Tx coils and the other four coils couple with Rx coils. The couplings between the MSR and Rxs could be chosen to be larger than the couplings between the MSR and Txs to reduce the resonator coil size, which is not limited by bifurcation phenomena. However, it is hard to achieve these high couplings via conventional coils of IPT systems, so high frequency coupled inductors (HFCI) can be used as both Rxs and the MSR are in the same rotating frame. In HFCI design, PQ32x20 with N87 material with an air gap of 0.4 mm was found to be the optimum magnetic core. The finalized HFCI parameters are presented in Table III.

B. System Tests

Several operating conditions are tested with the given experimental setup. The healthy operation of the system is verified at first. Then faulty conditions are tested. Detailed results are discussed in the following sections.

1) Normal Operation: Firstly, the system is operated at 156 kHz, slightly above the resonant frequency, which satisfies the zero voltage switching. The experimental results under normal operation are given in Fig. 12. The Rx currents are nearly equal and have a third harmonic component. The reflected third harmonic component can also be seen at the resonator current. Resonator currents are slightly smaller than the Tx current in experimental results due to the losses, which are not included in the analytical model.

TABLE II
EXPERIMENTAL SETUP PARAMETERS

Tx side MOSFET	BSC600N25NS3G
Tx side Gate Driver	2EDF7275F
Rx side Recrifier Diodes	C3D10060G
Litz Wire	400x0.08 mm (2 mm^2)
Ferrite shield	I20x2 N48
Tx coil D_{in} and D_{out}	70-280 mm
Tx coil # of turns	13
Tx coil inductances	83.1-83.5 μH
Resonator IPT coil D_{in} and D_{out}	65-280 mm
Resonator IPT coil # of turns	5
Resonator IPT coil inductance	23 μH
C_{Tx}	13.6 nF
C_R	15.21 nF
C_{Rx}	44.2 nF
Airgap	10 (mm)
Resonant frequency (f_0)	150 kHz
Operating frequency (f)	155 kHz

TABLE III
PARAMETERS OF THE HIGH FREQUENCY COUPLED INDUCTORS

Parameters	$HFCI_1$	$HFCI_2$	$HFCI_3$	$HFCI_4$
$L_R(\mu H)$	13.37	13.27	13.19	13.25
$L_{Rx}(\mu H)$	26.88	26.85	26.89	27.07
$M(\mu H)$	18.05	18.14	18.01	18.09
Core Size		PQ 35x35		
Core Material		N87		
Airgap		0.4 mm		
Number of R Turns		6		
Number of Rx Turns		9		

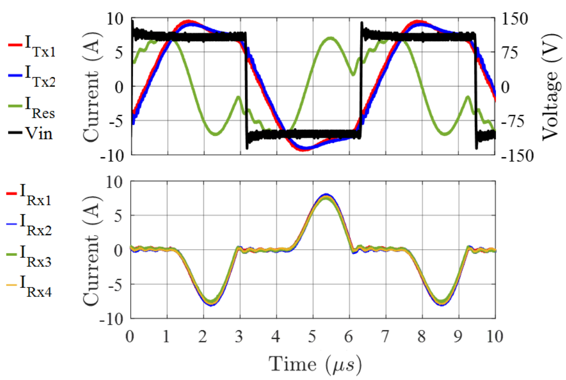

Fig. 12. Input voltage, Tx side currents, resonator current and Rx currents for healthy operation. ($I_{Tx1,2} \approx 6.5\ A_{rms}, I_R = 5.4\ A_{rms}$)

2) Single and Double Rx Open Circuit Fault: In Fig. 13.a, operation under a single Rx open circuit fault is presented. Results are similar to healthy operation, and the third harmonic component is reduced compared to the healthy operation. Since Rxs are over-designed in the experimental setup, the rated power is transferred; otherwise, the transferred power should be reduced as presented in (21). Increasing the number of Rx modules will result in less stress on the remaining modules under fault; however, it also increases the chance of a failure due to the increased number of components. Then the effect of simultaneous faults in two Rx modules is investigated. The results are presented in Fig. 13.b. The effective quality factor of the Rx modules becomes greater than healthy operation since the current of the remaining modules increases. Hence, the system operates in CCM, and the third harmonic is almost diminished.

3) Single Tx Open Circuit Fault: Finally, the fault tolerance of the system is tested with a single open circuit Tx fault. As the Tx modules are not over-designed, the power is reduced from 1000W to 250W, as shown in Fig. 13.c.

Under an open-circuited Tx fault, the flux linkage is reduced by half, which also decreases the resonator current, but the power is shared between the Rx modules equally. The rated power could be transferred if Tx modules are over-designed.

4) Efficiency under fault: The system efficiencies under healthy and faulty operations are given in Table IV. Single-Tx fault's efficiency is lower than healthy operation due to lower input voltage as expected. However, Txs have the same voltage and current value in single-Rx and double-Rx faults, providing compatible efficiency with the healthy operation, which confirms the fault tolerance of the proposed system.

TABLE IV
EFFICIENCIES OF THE SYSTEM UNDER HEALTHY AND FAULTY OPERATIONS

Operation	Efficiency
Healthy operation	90.9 %
Single Rx open faulty operation	89.6 %
Double Rx open faulty operation	89.5 %
Single Tx faulty operation	81.6 %

VII. CONCLUSION

This paper proposes a multi-Tx/multi-Rx system as an alternative to conventional slip rings for field excited synchronous machines. Thus, fault-tolerant and maintenance-free contactless slip rings are achieved. However, multi-Tx/multi-Rx systems are prone to unequal power-sharing between modules, reducing reliability. Therefore, a novel solution, introducing a middle-stage resonator, is presented to improve unequal power-sharing. Furthermore, the efficiency competing with the conventional slip rings is achieved by avoiding bifurcation, which guarantees zero voltage switching. In this paper, firstly, the design methodology of a multi-Tx/multi-Rx IPT system with a middle-stage resonator was presented. Then, a fault tolerance analysis was examined, and the selection of modules number was discussed. Finally, a 1 kW 2Tx/1MSR/4Rx prototype was built to validate the proposed system, and it was observed that the experimental results are coherent with analytical results under single-Rx, double-Rx, and single-Tx faults. Consequently, a fault-tolerant multi-Tx/ multi-Rx IPT system to excite the field of synchronous machines is achieved, decreasing maintenance requirements and increasing reliability.

REFERENCES

[1] O. Knecht and J. W. Kolar, "Performance evaluation of series-compensated ipt systems for transcutaneous energy transfer," *IEEE Transactions on Power Electronics*, vol. 34, no. 1, pp. 438–451, 2019.

[2] L. Chen, G. R. Nagendra, J. T. Boys, and G. A. Covic, "Double-coupled systems for ipt roadway applications," *IEEE Journal of Emerging and Selected Topics in Power Electronics*, vol. 3, no. 1, pp. 37–49, 2015.

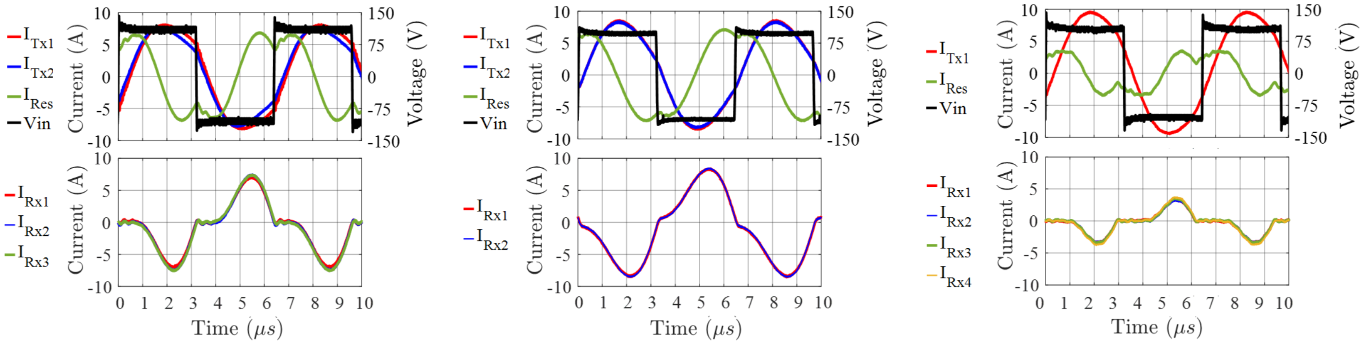

(a) (b) (c)

Fig. 13. The waveforms of input voltage, Tx side currents, resonator current and Rx currents for faulty operations. a) Single open circuited Rx fault. b) Double open circuited Rx fault. c) Single open circuited Tx fault.

[3] D. Wang, X. Qu, Y. Yao, and P. Yang, "Hybrid inductive-power-transfer battery chargers for electric vehicle onboard charging with configurable charging profile," *IEEE Transactions on Intelligent Transportation Systems*, vol. 22, no. 1, pp. 592–599, 2021.

[4] X. Qu, H. Chu, S.-C. Wong, and C. K. Tse, "An ipt battery charger with near unity power factor and load-independent constant output combating design constraints of input voltage and transformer parameters," *IEEE Transactions on Power Electronics*, vol. 34, no. 8, pp. 7719–7727, 2019.

[5] S. Mehri, A. C. Ammari, J. B. H. Slama, and M. Sawan, "Design optimization of multiple-layer pscs with minimal losses for efficient and robust inductive wireless power transfer," *IEEE Access*, vol. 6, pp. 31 924–31 934, 2018.

[6] Y. Zhang, S. Chen, X. Li, and Y. Tang, "Design methodology of free-positioning nonoverlapping wireless charging for consumer electronics based on antiparallel windings," *IEEE Transactions on Industrial Electronics*, vol. 69, no. 1, pp. 825–834, 2022.

[7] M. G. S. Pearce, G. A. Covic, and J. T. Boys, "Robust ferrite-less double d topology for roadway ipt applications," *IEEE Transactions on Power Electronics*, vol. 34, no. 7, pp. 6062–6075, 2019.

[8] W. Zhong, C. K. Lee, and S. Y. R. Hui, "General analysis on the use of tesla's resonators in domino forms for wireless power transfer," *IEEE Transactions on Industrial Electronics*, vol. 60, no. 1, pp. 261–270, 2013.

[9] G. Ke, Q. Chen, W. Gao, S.-C. Wong, C. K. Tse, and Z. Zhang, "Research on ipt resonant converters with high misalignment tolerance using multicoil receiver set," *IEEE Transactions on Power Electronics*, vol. 35, no. 4, pp. 3697–3712, 2020.

[10] L. Tian, F. Yang, B. Cai, S. Li, K. Liu, and H. Zhao, "High misalignment tolerance in efficiency of wpt system with movable intermediate coil and adjustable frequency," *IEEE Access*, vol. 9, pp. 139 527–139 535, 2021.

[11] L. J. Chen, G. R. Nagendra, J. T. Boys, and G. A. Covic, "Double-coupled systems for roadway ipt systems," in *2014 IEEE Applied Power Electronics Conference and Exposition - APEC 2014*, 2014, pp. 1618–1625.

[12] S. Moon and G.-W. Moon, "Wireless power transfer system with an asymmetric four-coil resonator for electric vehicle battery chargers," *IEEE Transactions on Power Electronics*, vol. 31, no. 10, pp. 6844–6854, 2016.

[13] Z. Wang, X. Cao, Y. Zhu, Y. Zhu, Q. Cai, and J. Fan, "Five-coil wireless charging structure with radiated slots in uavs for mutual inductance reduction," in *2021 International Applied Computational Electromagnetics Society (ACES-China) Symposium*, 2021, pp. 1–2.

[14] Q. Deng, Z. Li, J. Liu, S. Li, D. Czarkowski, M. K. Kazimierczuk, H. Zhou, and W. Hu, "Multi-inverter phase-shifted control for ipt with overlapped transmitters," *IEEE Transactions on Power Electronics*, vol. 36, no. 8, pp. 8799–8811, 2021.

[15] J. M. Arteaga, S. Aldhaher, G. Kkelis, C. Kwan, D. C. Yates, and P. D. Mitcheson, "Dynamic capabilities of multi-mhz inductive power transfer systems demonstrated with batteryless drones," *IEEE Transactions on Power Electronics*, vol. 34, no. 6, pp. 5093–5104, 2019.

[16] F. Lu, H. Zhang, H. Hofmann, and C. C. Mi, "A dynamic charging system with reduced output power pulsation for electric vehicles," *IEEE Transactions on Industrial Electronics*, vol. 63, no. 10, pp. 6580–6590, 2016.

[17] T.-S. Lee, S.-J. Huang, S.-H. Dai, and J.-L. Su, "Design of misalignment-insensitive inductive power transfer via interoperable coil module and dynamic power control," *IEEE Transactions on Power Electronics*, vol. 35, no. 9, pp. 9024–9033, 2020.

[18] H. Li, Y. Liu, K. Zhou, Z. He, W. Li, and R. Mai, "Uniform power ipt system with three-phase transmitter and bipolar receiver for dynamic charging," *IEEE Transactions on Power Electronics*, vol. 34, no. 3, pp. 2013–2017, 2019.

[19] H. Chen, Z. Qian, R. Zhang, Z. Zhang, J. Wu, H. Ma, and X. He, "Modular four-channel 50 kw wpt system with decoupled coil design for fast ev charging," *IEEE Access*, vol. 9, pp. 136 083–136 093, 2021.

[20] Q. Deng, P. Sun, W. Hu, D. Czarkowski, M. K. Kazimierczuk, and H. Zhou, "Modular parallel multi-inverter system for high-power inductive power transfer," *IEEE Transactions on Power Electronics*, vol. 34, no. 10, pp. 9422–9434, 2019.

[21] H. Zhou, J. Chen, Q. Deng, F. Chen, A. Zhu, W. Hu, and X. Gao, "Input-series output-equivalent-parallel multi-inverter system for high-voltage and high-power wireless power transfer," *IEEE Transactions on Power Electronics*, vol. 36, no. 1, pp. 228–238, 2021.

[22] G. Ning, K. Zhao, and M. Fu, "A passive current sharing method for multitransmitter inductive power transfer systems," *IEEE Transactions on Industrial Electronics*, vol. 69, no. 5, pp. 4617–4626, 2022.

[23] H. Hu, S. Duan, T. Cai, and P. Zheng, "A current-sharing compensation method for high-power-medium-frequency coils composed of multiple branches connected in parallel," *IEEE Transactions on Industrial Electronics*, vol. 69, no. 5, pp. 4637–4651, 2022.

[24] G. Ke, Q. Chen, W. Gao, S.-C. Wong, C. K. Tse, and Z. Zhang, "Research on ipt resonant converters with high misalignment tolerance using multicoil receiver set," *IEEE Transactions on Power Electronics*, vol. 35, no. 4, pp. 3697–3712, 2020.

[25] C.-S. Wang, G. Covic, and O. Stielau, "Power transfer capability and bifurcation phenomena of loosely coupled inductive power transfer systems," *IEEE Transactions on Industrial Electronics*, vol. 51, no. 1, pp. 148–157, 2004.

[26] K. Aditya and S. S. Williamson, "Design guidelines to avoid bifurcation in a series-series compensated inductive power transfer system," *IEEE Trans. Ind. Electron.*, vol. 66, no. 5, pp. 3973–3982, 2019.

[27] D. Patil, M. K. McDonough, J. M. Miller, B. Fahimi, and P. T. Balsara, "Wireless power transfer for vehicular applications: Overview and challenges," *IEEE Transactions on Transportation Electrification*, vol. 4, no. 1, pp. 3–37, 2018.

[28] V. Shevchenko, O. Husev, R. Strzelecki, B. Pakhaliuk, N. Poliakov, and N. Strzelecka, "Compensation topologies in ipt systems: Standards, requirements, classification, analysis, comparison and application," *IEEE Access*, vol. 7, pp. 120 559–120 580, 2019.

[29] H. Polat, "1kw contactless slip ring design using series-series resonant converter topology," Master's thesis, Middle East Technical University, 2021.

[30] Y. Fang, B. M. H. Pong, and R. S. Y. Hui, "An enhanced multiple harmonics analysis method for wireless power transfer systems," *IEEE Trans. Power Electron.*, vol. 35, no. 2, pp. 1205–1216, 2020.

[31] X. Qu, Y. Jing, J. Lian, S. Wong, and C. K. Tse, "Design for continuous-current-mode operation of inductive-power-transfer converters with load-independent output," *IET Power Electronics*, vol. 12, no. 10, pp. 2458–2465, 2019.